ABCM40 anos
Associação Brasileira de Engenharia e Ciências Mecânicas
CONEM 2016
CONGRESSO NACIONAL DE ENGENHARIA MECÂNICA
21 - 25 AGOSTO DE 2016
FORTALEZA - CEARÁ

Polynomial Chaos-based analysis of Multirotor Aerial Vehicles Model Subjected to Uncertainties

Nome do primeiro autor, e-mail[1]
Nome do segundo autor, e-mail[1]
Nome do terceiro autor, e-mail[2]

[1]Nome da instituição, endereço para correspondência
[2]Nome da instituição, endereço para correspondência
CON-2016-1213

Abstract: *Uncertainties are ubiquitous in mathematical equations that represent physical models and may come from unknown plant parameters or from the purposeful choice of a simplified representation of the system dynamics. In case of Multirotor Aerial Vehicles (MAVs), which have become interesting for applications where manned operations are considered inefficient and dangerous for humans, uncertainties such as inaccurate parameters, neglect of gyroscopic effect, blade flapping, as well as, wind gusts can have strong adverse effects on the system behavior. This paper uses the Polynomial Chaos Expansion method to propagate uncertainties in the multirotor model and characterize the effects over the vehicle trajectory, considering constraints on both the total thrust magnitude and the inclination of the rotor plane in the design of the position control. The Polynomial Chaos method constructs meta-models that accurately mimic the behavior of systems with uncertainty about the mean of stochastic inputs. The uncertainties are described in terms of normal distribution. The results are compared with Monte Carlo simulations.*
Keywords: *Uncertainty, Polynomial Chaos, Multirotor Aerial Vehicles*

1. INTRODUCTION

Among the different types of UAVs such as blimps (Elfes *et al.*, 1998), fixed-wings (Beard *et al.*, 2005) and rotary wings aircrafts (Bouabdallah *et al.*, 2004), we highlight the multirotors (Gupte *et al.*, 2012; Er *et al.*, 2013). The multirotor-type unmanned aerial vehicle (MAVs) technology has attracted a great deal of interest of the academia and industry and, consequently experienced a rapid improvement. This interest is justified by features such as their simplified mechanics, low cost, high maneuverability, and vertical take-off and landing (VTOL) capability. Examples of their applications are found in building exploration (Achtelika *et al.*, 2008), forest-fire monitoring (Alexis *et al.*, 2012) and mapping of agricultural areas (Barrientos *et al.*, 2011).

Although there is a massive amount of concluded and ongoing research works on multirotor helicopters, the design of control laws for such vehicles still has challenges to be overcome. Recently, more efforts have been directed toward the research of dealing with uncertainties associated with MAVs dynamics (Ton and MacKunis, 2012; Zhao *et al.*, 2014). However, a good robust control design requires a deep understanding about the effects caused by the presence of uncertainties

Uncertainty quantification (UQ) is the characterization of the effects of uncertainties on simulation or theoretical models of actual systems. Sources of uncertainty include parametric model perturbations, lack of physical fidelity of models, and uncertain circumstances in system operation (Sandoval *et al.*, 2012). The UQ can provide important information and perspectives for robust design and optimization and can be used to characterize the robustness, reachability and controllability of the system. Furthermore, in the presence of multiple sources of uncertainty, efficient robust control requires analyses of their relative impacts on certain system performance and behavior (Kim *et al.*, 2013).

Much research effort has been devoted to developing UQ methods. One of the well-known dynamic sampling methods is Monte Carlo simulation. This approach typically involves the analysis of a large number of simulations runs of an analytical or numerical system model with various combinations of parameters (Kewlani *et al.*, 2012). However, to ensure representation of the entire parameter range, a large number of simulations must be performed, often resulting in extensive computational costs. More recent approaches to stochastic simulation of processes subject to uncertainty include Polynomial Chaos Expansion (PCE) approach, which was originally introduced by Wienner (1938). PCEs have

become broadly used in a wide variety of fields including in stochastic differential equations (Xiu and Karniadakis, 2002), fluid dynamics (Walters, 2003), aircraft operations (Roberts *et al.*, 2011), robust design problems (Dodson and Parks, 2009). This approach can be considered as a spectral method to construct finite-dimensional approximations in infinite-dimensional probability measure space.

When constraints must be considered, model predictive control (MPC) algorithms appear as an interesting choice. The MPC is a strategy wherein a future control sequence is obtained by minimizing a cost function based on predictions of the controlled output along a finite horizon typically, subject to constraints (Camacho and Bordons, 1998). Recently, Prado and Santos (2014) tackled the problem of controlling the position of a multirotor while respecting constraints on the inclination of the rotor plane and on the magnitude of the total thrust vector. The present paper proposes to use the PCE to make the uncertainty quantification of a MAV position control designed by Prado and Santos (2014) considering the presence of wind gust with normal distribution. The disturbance effects are propagated to the outputs.

2. MAV MATHEMATICAL MODEL

This section presents the equations of motion of a multirotor aerial vehicle (MAV), considering all the relevant effects necessary to be accounted for in ground-thruth model for simulation-based evaluation of control laws. We start with preliminary definitions in Subsection 2.1, then we present the rotor dynamics in 2.2 and the MAV rotational dynamics in 2.3.

2.1 Preliminary definitions

We define two Cartesian coordinate systems (CCS) as illustrated in Fig. 1. The body CCS, $S_{\mathrm{B}} \triangleq \{X_{\mathrm{B}}, Y_{\mathrm{B}}, Z_{\mathrm{B}}\}$ is attached to the vehicle's body with the origin at the vehicle's center of mass (CM), the X_{B} axis pointing forward, the Z_{B} axis pointing upward, perpendicular to the plane of the rotors, and the Y_{B} axis completing a dextrogeous frame. The CCS, $S_{\mathrm{G}} = \{X_{\mathrm{G}}, Y_{\mathrm{G}}, Z_{\mathrm{G}}\}$ is fixed to the ground at a known point O, with the Z_{G} axis pointing upward, aligned with the local vertical.

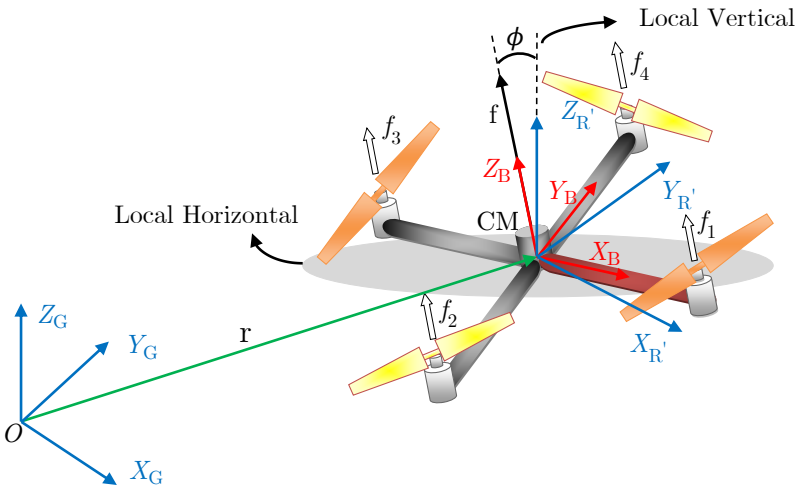

Figura 1: The Cartesian coordinate systems (CCS). $S_{\mathrm{B}} = \{X_{\mathrm{B}}, Y_{\mathrm{B}}, Z_{\mathrm{B}}\}$ is the body CCS and $S_{\mathrm{G}} = \{X_{\mathrm{G}}, Y_{\mathrm{G}}, Z_{\mathrm{G}}\}$ is the ground CCS.

2.2 Rotor dynamics

The thrust force f_i and reaction torque τ_i produced by each individual rotor are modeled, respectively, by the aerodynamic models (Mahony *et al.*, 2012)

$$f_i = k_f \omega_i^2, \tag{1}$$

$$\tau_i = k_\tau \omega_i^2, \tag{2}$$

for $i = 1, ..., 4$, where k_f is the force coefficient, k_τ is the torque coefficient, and ω_i is the rotation speed of the ith rotor (positive in courterclockwise direction), whose dynamics can be modeled by the following first-order linear model:

$$\dot{\omega}_i = -\frac{1}{\tau_\omega}\omega_i + \frac{k_\omega}{\tau_\omega}\bar{\omega}_i \tag{3}$$

where $\bar{\omega}_i \in [0, \bar{\omega}_{\max}]$ is the rotation speed command for the ith rotor, k_ω is the rotation coefficient, and τ_ω is rotor time constant.

2.3 Resultant control thrust and torque

Although the formulation given here could be generalized to any multirotor vehicle configuration, for illustration purpose, we consider a quadrotor configuration with the longitudinal axis X_{B} pointing between rotor 1 and rotor 2, and with 45 degree of separation angle between adjacent arms; we call it the "x"configuration. Moreover, we consider that rotor 1 and rotor 3 rotate in clockwise direction, while rotor 2 and rotor 4 rotate in counterclockwise direction. For the aforementioned configuration, one can show that the relationship between the individual rotor thrusts f_i and the resultant thrust magnitude and torque vector is given by

$$\begin{bmatrix} F^c \\ \mathbf{T}^c \end{bmatrix} = \mathbf{\Gamma f}, \tag{4}$$

with $\mathbf{f} \triangleq \begin{bmatrix} f_1 & f_2 & f_3 & f_4 \end{bmatrix}^{\mathrm{T}}$ and

$$\mathbf{\Gamma} \triangleq \begin{bmatrix} 1 & 1 & 1 & 1 \\ l/\sqrt{2} & -l/\sqrt{2} & -l/\sqrt{2} & l/\sqrt{2} \\ -l/\sqrt{2} & -l/\sqrt{2} & l/\sqrt{2} & l/\sqrt{2} \\ k_\tau/k_f & -k_\tau/k_f & k_\tau/k_f & -k_\tau/k_f \end{bmatrix}, \tag{5}$$

where l is the length of each vehicle's arm. The superscript c in Eq. (5) stands for the control command defined by the operator and is used to distinguish from the other sources of force and torque that will be presented soon.

By inverting Eq. (5), one can compute the command $\bar{\mathbf{f}} \triangleq \begin{bmatrix} \bar{f}_1 & \bar{f}_2 & \bar{f}_3 & \bar{f}_4 \end{bmatrix}^{\mathrm{T}}$ as

$$\bar{\mathbf{f}} = \Xi \begin{bmatrix} \bar{F}^c \\ \bar{\mathbf{T}}^c \end{bmatrix}, \tag{6}$$

where $\Xi \triangleq \Gamma^{-1}$, $\bar{F}^c$ is the thrust magnitude command, and $\bar{\mathbf{T}}^c$ is the control torque command.

2.4 Rotational motion

Representing the attitude using the Euler angles $\boldsymbol{\alpha} \triangleq \begin{bmatrix} \phi & \theta & \psi \end{bmatrix}^{\mathrm{T}}$ in the rotation sequence 1-2-3, we have the following rotational kinematics equations:

$$\dot{\boldsymbol{\alpha}} = \mathcal{A}\mathbf{\Omega} \tag{7}$$

where $\mathbf{\Omega} \triangleq [\Omega_x \ \Omega_y \ \Omega_z]^{\mathrm{T}}$ is the S_{B} representation of the vehicle's angular velocity w.r.t. S_{G} and

$$\mathcal{A} \triangleq \begin{bmatrix} \cos\psi/\cos\theta & -\sin\psi/\cos\theta & 0 \\ \sin\psi & \cos\psi & 0 \\ -\cos\psi\sin\theta/\cos\theta & \sin\psi\sin\theta/\cos\theta & 1 \end{bmatrix} \tag{8}$$

Assume that the vechile has a rigid structure and S_{G} is an inertial frame. Considering the existence of gyroscopic effects, due to the rotors, and disturbance torques, and using the Newton-Euler formulation, one can model the rotational dynamics of the MAV by

$$\dot{\mathbf{\Omega}} = \mathbf{J}^{-1}(\mathbf{J}\mathbf{\Omega}) \times \mathbf{\Omega} + I_r\mathbf{J}^{-1}\mathbf{\Omega} \times \mathbf{e}_3 \sum_{i=1}^{4} (-1)^i \omega_i + \mathbf{J}^{-1}\mathbf{T}^c + \mathbf{J}^{-1}\mathbf{T}^d \tag{9}$$

where $\mathbf{T}^c$ and $\mathbf{T}^d$ are the S_{B} representations of the resultant control torque and disturbance torque, respectively, $\mathbf{e}_3 \triangleq [0 \ 0 \ 1]^{\mathrm{T}}$, I_r is the moment of inertia of the rotors w.r.t. the rotation axis, and $\mathbf{J}$ is the body inertia matrix. Consider that the vehicle has a symmetric structure with known mass m and inertia matrix in S_{B}

$$\mathbf{J} = \begin{bmatrix} J_x & 0 & 0 \\ 0 & J_y & 0 \\ 0 & 0 & J_z \end{bmatrix}. \tag{10}$$

This paper makes use of the AR Drone 2 parameters in order to emulate a real plataform. The values can be seen in Table 1.

2.5 Translational motion

Consider that the Earth is flat and the gravitational acceleration g is constant anywhere the vehicle is supposed to operate. Therefore, the S_{G} representation of the gravitational acceleration vector is given by

$$\mathbf{g} = \begin{bmatrix} 0 \\ 0 \\ -g \end{bmatrix}. \tag{11}$$

Tabela 1: Parameters of AR Drone 2.

Variables	Values	Unit
Mass of AR Drone 2, m	0.429	kg
Acceleration of gravity, g	9.80665	$\mathrm{m/s^2}$
Arm lenght, l	0.1785	m
Moment of inertia for x-axis, J_x	2.238×10^{-3}	$\mathrm{kg.m^2}$
Moment of inertia for y-axis, J_y	2.986×10^{-3}	$\mathrm{kg.m^2}$
Moment of inertia for z-axis, J_z	4.804×10^{-3}	$\mathrm{kg.m^2}$
Moment of inertia of each rotor, I_r	2.030×10^{-5}	$\mathrm{kg.m^2}$
Force coefficient k_f	8.050×10^{-6}	$\mathrm{N/(rad/s)^2}$
Torque coefficient, k_τ	2.423×10^{-7}	$\mathrm{N.m/(rad/s)^2}$
Time constant, τ_ω	4.718×10^{-3}	s
Maximum speed of the motor, $\omega_{\max}$	1047	rad/s

Denote the S_{G} representations of the position and velocity of S_{B} w.r.t. S_{G} by $\mathbf{r} = [r_x\ r_y\ r_z]^{\mathrm{T}}$ and $\mathbf{v} = [v_x\ v_y\ v_z]^{\mathrm{T}}$, respectively. Therefore we can describe the vehicle's translational kinematics and dynamics by

$$\dot{\mathbf{r}} = \mathbf{v}, \tag{12}$$

$$\dot{\mathbf{v}} = \frac{F^c}{m}\mathbf{n} + \mathbf{g} + \frac{1}{m}\mathbf{F}^d, \tag{13}$$

where $\mathbf{n} \triangleq [\ \sin\phi \quad -\sin\phi\cos\theta \quad \cos\phi\cos\theta\ ]^{\mathrm{T}}$ is the S_{G} representation of the unit vector perpendicular to the plane of the rotors, $\mathbf{F}^d$ is the S_{G} representation of the disturbance force, m is the vehicle's total mass, and F^c is the magnitude of the resultant control thrust.

3. MODEL PREDICTIVE CONTROLLER

The present work faces the problem of safely controlling the position trajectory of multirotor UAVs by taking into consideration a conic constraint on the total thrust vector (see Fig 2a) and considering the presence of disturbance forces $\mathbf{F}^d$. The problem is solved using a linear state-space model predictive control (MPC) strategy, whose optimization is made handy by replacing the original conic constraint set on the thrust vector by an inscribed pyramidal space (see Fig 2b), which renders a linear set of inequalities. The control vector computed by the MPC is converted into a thrust magnitude command and an attitude command. For more details about control strategy, consult the reference Prado and Santos (2014).

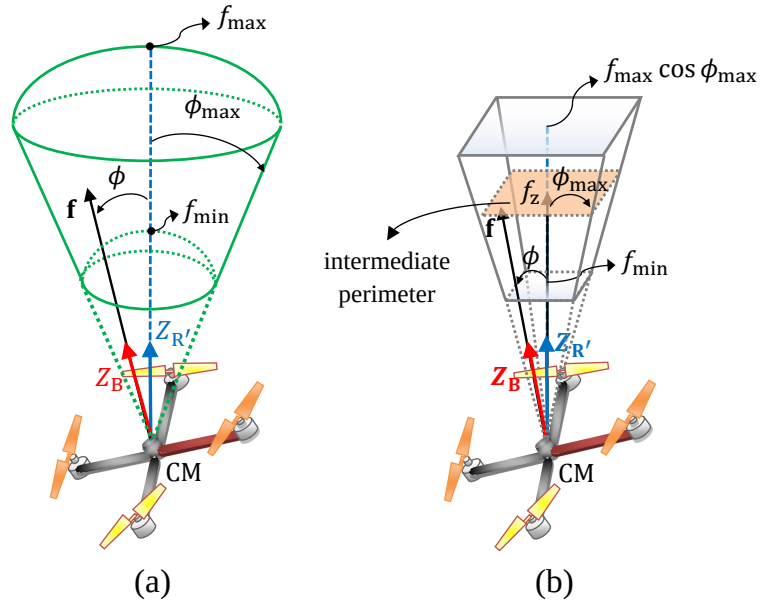

Figura 2: (a) Original constraints space; (b) Linearized constraints space.

The constraints on both magnitude and inclination of $\mathbf{f}$ are directly connected to the vertical and lateral accelerations of the vehicle. As one can see in Fig. 3, the component f_{z} is responsible for controlling the altitude of the vehicle, while $\mathbf{f}_{\mathrm{xy}}$ produces the lateral acceleration that leads the vehicle along the X_{R} and Y_{R} directions, where $\mathbf{f}_{\mathrm{xy}} \triangleq [f_{\mathrm{x}}\ f_{\mathrm{y}}]^{\mathrm{T}} \in \mathbb{R}^2$ denotes the horizontal projection of $\mathbf{f}$. As ϕ increases, the lateral acceleration of the vehicle increases. On the other hand, if the constraint $f_{\max}$ is not sufficiently high, the vehicle could suffer loss of lift. Furthermore, it is interesting to choose an $\phi_{\max}$ that avoids unexpected flips of the vehicle.

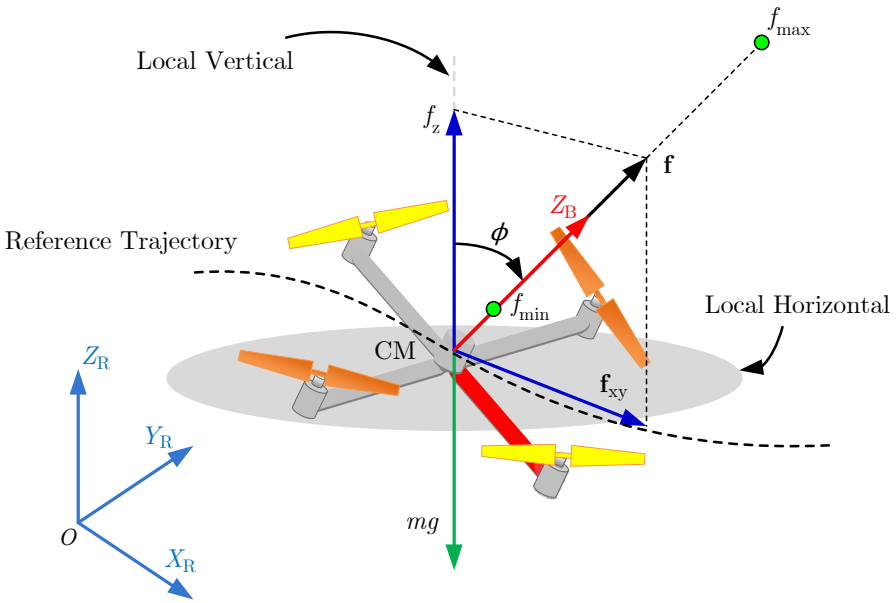

Figura 3: Analysis of **f** with respect to its constraints on inclination and magnitude.

4. POLYNOMIAL CHAOS EXPANSION

The analysis of uncertainty propagation and quantification in models has several appliacations in systems engineering. In the presence of stochastic uncertainties, it is important to determine the probabilities of the system properties exceeding specified critical values or operation limits, and such evaluation can be used to conduct reliability and risk analyses. In order to quantify the effects of the disturbance forces $\mathbf{F}^d$ on the vehicle trajectory, we employ the nonintrusive formulation of the polynomial chaos expansion in terms of the multivariate Hermite polynomials. The approach considers the analysis of stochastic system responses and uses the PCE as a functional approximation of the mathematical model.

According to Wiener, a stochastic process can be represented through a spectral expansion using orthogonal polynomials (Hermite polynomials) as (Sandoval *et al.*, 2012)

$$g(t,\boldsymbol{\xi}) = \sum_{j=0}^{\infty} g_j(t)\Psi_j(\boldsymbol{\xi}) \tag{14}$$

where $g_j(t)$ is the corresponding deterministic coefficient to be calculated from a limited number of model simulations, $\boldsymbol{\xi} = (\xi_1, \ldots, \xi_d)$ the d standard normal independent random variables with zero mean and unit standard deviation and Ψ_j the multivariate Hermite polynomials. In practice, the PCE (14) is truncated to a finite number of terms M. This number is denoted by

$$M = \frac{(p+d)!}{p!d!} - 1 \tag{15}$$

where p is the maximum order of the multivariate polynomial. It is worth noting that the required degree for the polynomial is not know a priori and must be tested to obtain the best accuracy. The multivariate polynomial $\Psi_j(\boldsymbol{\xi})$ is given by the tensor product of the corresponding one-dimensional Hermite polynomials $H_{\alpha_k^j}$

$$\Psi_j(\boldsymbol{\xi}) = \prod_{k=1}^{d} H_{\alpha_k^j}(\xi_k) \tag{16}$$

with α_k^j the degree of the one-dimensional Hermite polynomials, such that

$$|\alpha^j| = \sum_{k=1}^{d} \alpha_k^j \leq p, j = 0, ..., M. \tag{17}$$

An interesting result of the expansion present in Eq. 14 is that the first two statistical moments of the random variable g are computed from the terms of the PCE, with no need of Monte Carlo sampling methods. Considering the truncated decomposition, we have:

$$E[g(t,\boldsymbol{\xi})] = E\left[\sum_{j=0}^{M} g_j(t)\Psi_j(\boldsymbol{\xi})\right] = g_0(t) \tag{18}$$

$$V[g(t,\boldsymbol{\xi})] = V\left[\sum_{j=0}^{M} g_j(t)\Psi_j(\boldsymbol{\xi})\right] = \sum_{j=0}^{M} g_j^2(t)V\left[\Psi_j(\boldsymbol{\xi})\right] \tag{19}$$

Once the structure of the PCE is obtained for the model output, the deterministic coefficients $g_j(t)$ must be calculated. There exist two types of methods for this, the intrusive and the nonintrusive ones. The intrusive method requires to solve a system of coupled complex equations which could make the implementation of the PCE difficult or sometimes impossible. The nonintrusive approaches use interpolation methods and are very useful when trying to quantify uncertainty in complex stochastic models. The PC coefficients could be obtained through the regression of the mean-square optimization problem. Consider a sample of size N for the variable $g(t,\boldsymbol{\xi})$ and the parameters ξ_i with $i = 1,\ldots,d$, at each time instant, the coefficients $\hat{g}(t)$ are given by

$$\hat{g}(t) = (L^{\mathrm{T}}L)^{-1}L^{\mathrm{T}}g(t,\boldsymbol{\xi}) \tag{20}$$

where $\hat{g}(t)$ is the vector of PC coefficients at instant t and

$$L = \begin{bmatrix} \Phi_0(\xi_1) & \Phi_1(\xi_1) & \Phi_2(\xi_1) & \ldots & \Phi_M(\xi_1) \\ \Phi_0(\xi_2) & \Phi_1(\xi_2) & \Phi_2(\xi_2) & \ldots & \Phi_M(\xi_2) \\ \vdots & \vdots & \vdots & \vdots & \vdots \\ \Phi_0(\xi_d) & \Phi_1(\xi_d) & \Phi_2(\xi_d) & \ldots & \Phi_M(\xi_d) \end{bmatrix}. \tag{21}$$

We can represent the position components $r_x(t,\boldsymbol{\xi})$, $r_y(t,\boldsymbol{\xi})$, $r_z(t,\boldsymbol{\xi})$ and the control input signals provided by the MPC controller $\bar{F}^c(t,\boldsymbol{\xi})$ and $\bar{\phi}^c(t,\boldsymbol{\xi})$ by means of the PCE of order M according to Eqs. (14)-(16):

$$r_x(t,\boldsymbol{\xi}) \approx \sum_{j=0}^{M} r_{x,j}\,(t)\Psi_j(\boldsymbol{\xi}) \tag{22}$$

$$r_y(t,\boldsymbol{\xi}) \approx \sum_{j=0}^{M} r_{y,j}\,(t)\Psi_j(\boldsymbol{\xi}) \tag{23}$$

$$r_z(t,\boldsymbol{\xi}) \approx \sum_{j=0}^{M} r_{z,j}\,(t)\Psi_j(\boldsymbol{\xi}) \tag{24}$$

$$\bar{F}^c(t,\boldsymbol{\xi}) \approx \sum_{j=0}^{M} \bar{F}^c{}_{,j}\,(t)\Psi_j(\boldsymbol{\xi}) \tag{25}$$

$$\bar{\phi}^c(t,\boldsymbol{\xi}) \approx \sum_{j=0}^{M} \bar{\phi}^c{}_{,j}\,(t)\Psi_j(\boldsymbol{\xi}) \tag{26}$$

5. COMPUTATIONAL SIMULATIONS

The simulation is implemented in MATLAB/Simulink. The nonlinear 6DOF dynamics of a multirotor aerial vehicle is simulated using a 4th-order Runge-Kutta with a time step of 0.001s. This paper makes use of a more realistic MAV model than the one considered in Prado and Santos (2014). An exogenous disturbance $\mathbf{F}^d$ is considered during the simulation and it was modelled as follows

$$\mathbf{F}^d = \begin{bmatrix} (0.2 + 0.1\xi_1)\sin(\pi + 0.3\xi_3)t \\ (0.2 + 0.1\xi_2)\sin(\pi + 0.3\xi_4)t \\ (0.2 + 0.1\xi_3)\sin(\pi + 0.3\xi_6)t \end{bmatrix} \tag{27}$$

where ξ_i with $i = 1,\ldots,6$, as aforementioned, are random variables with zero mean and unit standard deviation. The vehicle is commanded to navigate through the following waypoints $\mathbf{r}_i = [1\ 1\ 0]^{\mathrm{T}}$, $\mathbf{w}_1 = [1\ 1\ 1]^{\mathrm{T}}$, $\mathbf{w}_2 = [2\ 1\ 1]^{\mathrm{T}}$, $\mathbf{w}_3 = [2\ 2\ 1]^{\mathrm{T}}$, $\mathbf{w}_4 = [1\ 2\ 1]^{\mathrm{T}}$, $\mathbf{w}_5 = [1\ 1\ 1]^{\mathrm{T}}$ with different combinations of reference speed v and maximum inclination angle $\phi_{\max}$. The polynomial chaos coefficients of the outputs and control signals were calculated considering 300 samples.

Tabela 2: Polynomial Chaos Results for Different Values of v and $\phi_{\max}$.

v [m/s]	$\phi_{\max}$ [deg]	RMSE(r_x) [m]	RMSE(r_y) [m]	RMSE(r_z) [m]	IADU(ϕ^c)	IADU(f)
0.5	10	0.2793	0.3582	0.0705	35.0596	8.2690
	20	0.2610	0.3300	0.0704	41.9833	8.9152
	30	0.2645	0.3322	0.0704	43.2785	7.9985
1.0	10	0.6421	0.6933	0.1242	27.9384	8.4848
	20	0.5557	0.6195	0.1234	48.9406	8.5728
	30	0.5479	0.6076	0.1233	43.6553	8.4185
2.0	10	0.7476	0.6696	0.2167	27.5862	9.7214
	20	0.6777	0.6573	0.2156	75.2982	9.1662
	30	0.6616	0.6512	0.2150	98.7541	9.0742

In order to make a quantitative comparison of the results attained by these combinations, two performace indexes have been computed. The Root Mean Square Error (RMSE) and the Integral Absolute Derivative Control Signal (IDAU) indexes obtained from the simulations results are presented in Table 2. One can see that as $\phi_{\max}$ increases, the RMSE(r_x) and RMSE(r_y) decreases. The same trend is observed in all the reference speeds. This behavior is explained by the fact that a smaller $\phi_{\max}$ implies in a lower horizontal acceleration (see Fig. 3), which in turn reduces the maneuverability of multirotor and consequently the vehicle is not able to reject the disturbance force quickly. As $\phi_{\max}$ increases, the horizontal component $\mathbf{f}_{\text{xy}}$ becomes higher, improving the maneuverability of the vehicle, which in turn provides a faster disturbance rejection. However, the RMSE(r_z) suffers less influence due to the fact that the vehicle's rotors have more freedom to produce vertical thrust. On the other hand, the IADU($\bar{\phi}^c$) had its value increased which shows that the increasing of $\phi_{\max}$ produces higher stress of the control actuator, while the values of the IADU($\bar{f}^c$) confirms that the altitude control effort is minimum, even when the vehicle is flying with $v = 2$ m/s and $\phi_{\max} = 30^o$.

Now, assigning a specific maximum inclination angle to the vehicle, for example $\phi_{\max} = 30^o$, and varying the reference speed v, one can see that the standard deviation envelope increases, as illustrated in Fig. 4. The main reason is the fact that restricting the maneuverability of the vehicle, it reduces the capability of producing horizontal acceleration.

Finally, it is possible to see that even using few samples of the system output, the PCE had a good performance and kept really close to the MC simulation graphs considering 1000 runs (see Fig. 4). Moreover, the computational cost of the PCE simulations considering 1000 runs was much lower when compared with the MC simulations, as illustrated in Table 3.

Tabela 3: Computational cost PCE $\times$ MC.

PCE [sec]	MC [sec]
255	6035

6. CONCLUSIONS

The control method proposed by Prado and Santos (2014) was evaluated by computational simulations considering that the vehicle was subjected to a random disturbance force process with amplitude and frequency described by random variables with normal distribution. One can conclude that the PCE method is able to propagate the effects of disturbance forces under the vehicle trajectory. Moreover, a rapid position command yields a larger variability on the system response and it is necessary to relax the maximum inclination constraint in order to have sufficient lateral control accelerations to overcome the disturbance forces. For future work, we intend to improve the disturbance model in order to consider effects of $\mathbf{T}^d$ into the rotational dynamics of the vehicle and analyze parametric uncertainties. Moreover, there is a growing interest in combining robust control approaches with stochastic control methods in order to be less conservative during the control design. Considering this motivation, we intend to design a probabilistic robust control strategies for a MAV.

7. ACKNOWLEDGEMENTS

The authors thank Coordenação de Aperfeiçoamento de Pessoal de Nível Superior (CAPES) and Conselho Nacional de Desenvolvimento Científico e Tecnológico (CNPq) for financial supports.

8. REFERENCES

Achtelika, M., Bachrachb, A., Heb, R., Prenticeb, S. and Roy, N., 2008. "Autonomous navigation and exploration of a quadrotor helicopter in gps-denied indoor environments". In *Science and Systems Conference*. Madrid, pp. 25–32.

Alexis, K., Nikolakopoulos, G., Tzes, A. and Dritsas, L., 2012. "Coordination of helicopter uav for aerial forest-fire surveillance". *Applications of Intelligent Control to Engineering Systems*, Vol. 39, pp. 169–193.

Barrientos, A., Colorado, J., del Cerro, J., Martinez, A., Rossi, C., Sanz, D. and Valente, J., 2011. "Aerial remote sensing

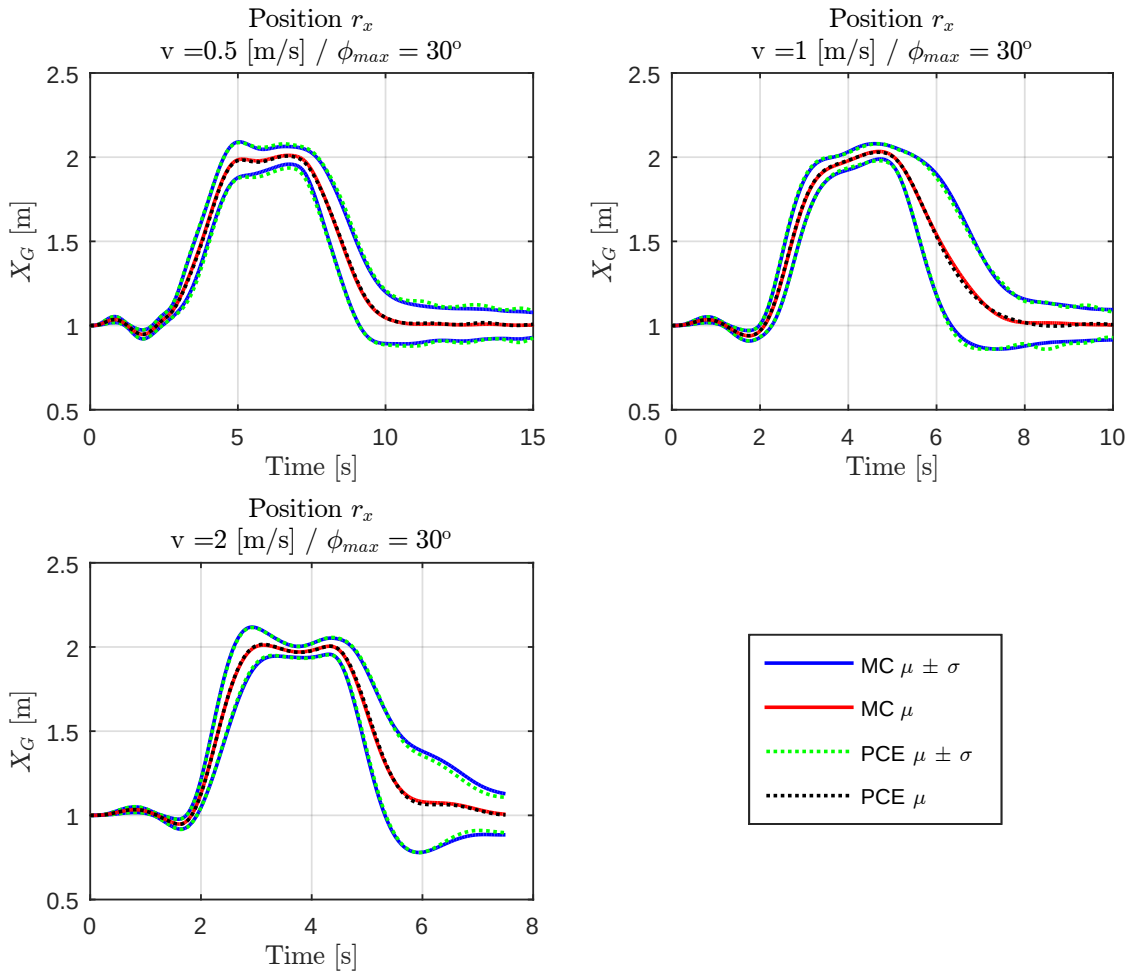

Figura 4: The standard deviation tunel along X_G axis.

in agriculture: a practical approach to area coverage and path planning for fleets of mini aerial robots". *Journal of Field Robotics*, Vol. 28, No. 5, pp. 667–689.

Beard, R., Kingston, D., Quigley, M., Snyder, D., Christiansen, R., Johnson, W., McLain, T. and Goodrich, M.A., 2005. "Autonomous vehicle technologies for small fixed-wing uavs". *Journal of Aerospace Computing, Information and Communication*, Vol. 30, pp. 92–108.

Bouabdallah, S., Murrieri, P. and Siegwart, R., 2004. "Design and control of an indoor micro quadrotor". In *Proceedings of the IEEE International Conference on Robotics and Automation*. New Orleans, pp. 4393–4398.

Camacho, E. and Bordons, C., 1998. *Model predictive control*. Spring-Verlag.

Dodson, M. and Parks, G.T., 2009. "Robust aerodynamic design optimization using polynomial chaos". *Journal of Aircraft*, Vol. 46, No. 2.

Elfes, A., Bueno, S.S., Bergerman, M. and Ramos, J.G., 1998. "A semi-autonomous robotic airship for environmental monitoring missions". In *Proceedings of the IEEE International Conference on Robotics and Automation*. Leuven, pp. 3449–3455.

Er, M.J., Yuan, S. and Wang, N., 2013. "Development control and navigation of octocopter". In *10th International Conference on Control and Automation*. Hangzhou, pp. 1639–1643.

Gupte, S., Mohandas, P.I.T. and Conrad, J.M., 2012. "A survey of quadrotor unmanned aerial vehicles". In *Proceedings of the IEEE Southeastcon*. Orlando, pp. 1–6.

Kewlani, G., Crawford, J. and Iagnemma, K., 2012. "A polynomial chaos approach to the analysis of vehicle dynamics under uncertainty". *International Journal of Vehicle Mechanics and Mobility*, Vol. 50, No. 5, pp. 749–774.

Kim, K.K.K., Shen, D.E., Nagy, Z.K. and Braatz, R.D., 2013. "Wiener's polynomial chaos for the analysis and control of nonlinear dynamical systems with probabilistic uncertainties". *IEEE Control Systems*, Vol. 33, No. 5, pp. 58–67.

Mahony, R., Kumar, V. and Corke, P., 2012. "Multirotor aerial vehicles: modeling, estimation, and control of quadrotor". *IEEE Robotics and Automation Magazine*, Vol. 19, No. 3, pp. 20–32.

Prado, I.A.A. and Santos, D.A., 2014. "A safe position tracking strategy for multirotor helicopters". In *22nd Mediterranean Conference on Control and Automation*. Palemo, pp. 1433–1439.

Roberts, B., Lind, R. and Kumar, M., 2011. "Polynomial chaos analysis of mav's in turbulence". In *AIAA Atmospheric Flight Mechanics Conference*. Oregon, p. 6214.

Sandoval, E.H., Collin, F.A. and Basset, M., 2012. "Sensitivity sutdy of dynamic systems using polynomial chaos". *Reliability Engineering and System Safety*, Vol. 104, No. 5, pp. 15–26.

Ton, C.T. and MacKunis, W., 2012. "Robust attitude tracking control of a quadrotor helicopter in the presence of uncertainty". In *51st IEEE Conference on Decision and Control*. Maui, pp. 937–942.

Walters, R.W., 2003. "Towards stochastic fluid mechanics via polynomial chaos". In *41st Aerospace Sciences Meeting and Exhibit*. Nevada, p. 0413.

Wienner, N., 1938. "The homogeneous chaos". *American Journal of Mathematics*, Vol. 60, No. 4, pp. 897–936.

Xiu, D. and Karniadakis, G.E., 2002. "The wiener-askey polynomial chaos for stochastic differential equations". *SIAM J. Sci. Comput.*, Vol. 24, No. 2, pp. 619–644.

Zhao, B., Xian, B., Zhang, Y. and Zhang, X., 2014. "Immersion and invariance based adaptive attitude tracking control of a quadrotor uav in the presence of parametric uncertainty". In *33rd Chinese Control Conference*. Nanjing, pp. 1932–1937.

9. RESPONSIBILITY NOTICE

The authors are the only responsible for the printed material included in this paper.